

Multiple Geometric surfaces detection in Geometric Coordination Registration for implant surgery virtual planning and assessment

Zhi-Jie Wu
School of Information Engineering
Guangdong University of Technology
Guangzhou, People's Republic of China
2111903078@mail2.gdut.edu.cn

Tai-Chiu Hsung*
Department of Computer Science
Chu Hai College of Higher Education
Hong Kong
ORCID: 0000-0001-7699-1937

Wing-Kuen Ling
School of Information Engineering
Guangdong University of Technology
Guangzhou, People's Republic of China
ORCID: 0000-0002-0633-7224

Cai-Yun Heng
Faculty of Dentistry
The University of Hong Kong
Hong Kong
clairehengheng51@gmail.com

Walter Yu-Hang Lam
Faculty of Dentistry
The University of Hong Kong
Hong Kong
ORCID: 0000-0001-5530-2645

Yu Pan
Faculty of Dentistry
The University of Hong Kong
Hong Kong
yupan@hku.hk

Abstract—Objective: The aim of this study is to develop automatic methods of geometric coordination registration (GCR) for the virtual planning and evaluation of implant surgery. **Methods:** The target modalities of the image to be registered are cone-beam computed tomography (CBCT) or optical surface (OS) scan. Several geometric fiducial markers, cubic corners (CC) and discs, are fabricated on the patient's oral stent and digitized into a 3D mesh model. By analyzing the distribution of vertices and normal vectors of the mesh model, a novel descriptor is proposed to detect the position of the geometric fiducial markers. CC edges and disc centers are then used to find the transformation matrix to align the input point cloud to the target Cartesian axes. **Results:** CBCT and OS scans of the plaster models with implants of 29 patients were collected. The implant positions found by using the proposed algorithm were compared to the Gold standard developed with a coordinate measuring machine (CMM). Experimental results show that the target registration error (TRE) of the proposed method was 0.43mm. **Conclusion:** The proposed method performs better than existing manual or semi-automatic GCR (TRE 0.52mm).

Keywords—registration, cone-beam computed tomography, optical scanner

I. INTRODUCTION

In oral implant surgery planning [1]-[6], surgeons usually perform trial operations on virtual or rapid prototype stereoscopic lithography models. The 3D images are CBCT [7] and OS [8] scans which are routinely performed in the diagnosis. The planning can now be done in the computer environment [9] completely, the planned physical surgical stents can be fabricated directly with 3D printing. During the planning and post-operation assessment, multiple images which possibly acquired from various imaging modalities are registered. As all the imaging modality exhibits different level of error during image acquisition [10], image to image (I/I) registration in pair does not give estimation of error to physical domain. It is further complicated with imaging error in each acquisition such as calibration errors. Therefore, a new geometric coordination registration for registering physical model and virtual image was proposed [11]. This enables simple linear and coordinate measurement of physical and virtual domain.

Lam et al. proposed to use cubic corners to align 3D images [11]-[13] to the Cartesian coordinate axes in computer

environment. The registration can perform mapping from physical to image (PI) or image to physical (IP), which is known as the “geometric coordination registration”. Further, it is suggested to adopt multiple flat surfaces [14] for IP/PI registration. It is particularly useful for registering serial 3D images at different time instances. These surfaces have an intrinsic relationship that defines the origin and axes of the cartesian coordinate system. The mean target registration errors (TRE) [15]-[16] achieved were $0.56 \pm 0.24\text{mm}$ and $0.39 \pm 0.21\text{mm}$ for manual and semi-automatic registration (SR) respectively on acrylic blocks. The shape of CC and discs enable easy identification in various imaging modalities and simple alignment to CMM for physical measurement, where the TRE of the registration can be directly calculated. However, current available methods for GCR is manual or semi-automatic, which are performed on computer software such as 3D slicer, MeshLab etc.

In this paper, the automation of detecting geometric fiducial marker for GCR is studied. It not only reduces registration errors, but also eliminates operator variability. In the next section, the data collection and overview of the proposed system is firstly described. Then, each step is detailed in section III. A new automatic detection method of geometric markers based on local normal vector distribution is proposed. This method was tested in 29 types of plaster models, each of which was implanted with plaster. The CMM is used to measure the position of the implant and serve as a benchmark gold standard. Experimental results show that the average TRE using semi-automatic and suggested automatic methods are 0.52mm and 0.43mm, respectively.

II. MATERIALS

Twenty-nine dentate subjects' maxillary stone models were collected and their right central incisors were removed. The models were duplicated into resin models. An implant (4.1*13mm, AstraTech EV, DENTSPLY) was inserted into each of these resin models to replace the central incisor. For each resin model, a full-arch heat-cure acrylic stent with a cubic corner (CC) [12] at the maxillary left central incisor region and two cylinders was fabricated (Fig.2). The superior surface of the CC and the surface of the two discs are made to be coplanar. The resin models with acrylic stents were then scanned with CBCT (Newtom GiANO), Intraoral scanner (Sirona Primescan), and a Lab scanner (3Shape D2000). 3D

mesh models are generated and preprocessed with the 3D slicer and MeshLab. They are saved in PLY or OBJ file format for further geometric coordination registration processing.

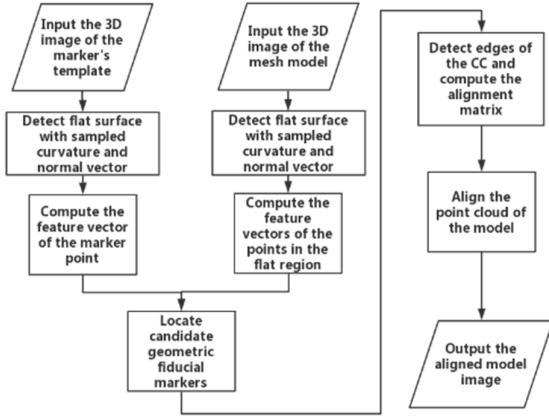


Fig. 1. System block diagram of the proposed automatic point cloud based geometric coordination registration.



Fig. 2. Maxillary teeth resin cast (yellow) with full-arch heat-cure acrylic stent (pink).

III. THE PROPOSED METHOD

The following is an outline of the proposed geometric coordination registration method, the detailed steps will be described in the next sections.

Algorithm 1 (Point cloud based Geometric Coordination Registration)

1. Detect flat surfaces $P_i^K = \{p_i^k: k = 1, \dots, K\}$ from input point cloud.
2. For each point p_i^k , compute the feature vector.
3. Locate candidate geometric fiducial markers by matching with template's feature vector.
4. Detect edges of the CC by intersecting lines of multiple planes, discs centers and compute the alignment matrix.
5. Align the point cloud of the model.

As shown in Fig.1, the proposed method starts from the detection of flat surfaces in the input point cloud. They are matched by comparing feature vector of the input point cloud and the precomputed templates, which are geometric fiducial markers CC and circular discs containing flat surfaces. 3D mesh models of the markers templates can be made using Computer Aided Design (CAD) [17] or mesh processing

software's such as MeshLab [18]. The feature vector is designed based on the characteristics of the local vertex patch. It is composed of the normal vector and the vertex position distribution. The calculation method is introduced in section B below. Denote the center point of the plane in axial direction (CC/discs) on the marker as $f_{template}$, as shown in Fig. 3(a) and Fig. 3(b). In Fig. 3(c), it shows the 3D mesh model of the resin model with acrylic stent of a patient. After the markers in the model are located, the position and orientation of the coordinate axis are determined according to the parallel or orthogonal relation of each plane of the markers. RANSAC algorithm is adopted to figure out each plane of the marker. There are several combinations of the references can be extracted from the markers for the final alignment to the coordinate axis: 1) The intersecting points and intersecting lines of the three orthogonal planes of the cube. 2) The upper planes of two posterior circular discs markers, which are physically made to be coplanar with the upper plane of the CC markers.

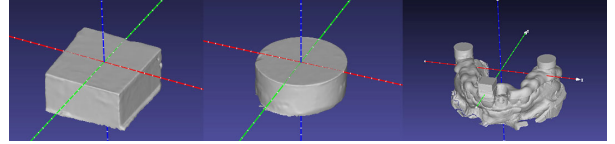


Fig. 3. 3D mesh model of geometric fiducial markers (a) CC and (b) circular discs. (c) Resin model with acrylic stent.

A. Flat surfaces detection

Without loss of generality, the input point clouds of the template and model contains flat surfaces only in the geometric markers, i.e., the CC and discs surfaces. They are detected by using local curvature value. As the input point clouds may contains a huge number of points, they are firstly downsampled to reduce computation cost. Denote as $P_{template} = \{p_i: i = 1, \dots, M\}$ and $P_{model} = \{p_j: j = 1, \dots, N\}$, where M and N are the number of downsampled point sets of $P_{template}$ and P_{model} . Then, Kd-trees [19] $T_{template}$ and T_{model} are built for $P_{template}$ and P_{model} . For each points in $P_{template}$ and P_{model} , a local patch of points selected for the computation of curvature. For each point p_i in $P_{template}$ and p_j in P_{model} , considered K nearest neighboring points $P_i^K = \{p_i^k: k = 1, \dots, K\}$ and $P_j^K = \{p_j^k: k = 1, \dots, K\}$. The covariance matrices Σ_i and Σ_j , and the associated eigenvalues $(\lambda_1, \lambda_2, \lambda_3)$ and eigenvectors (e_1, e_2, e_3) , are obtained for P_i^K and P_j^K respectively. The eigenvector corresponding to the minimum eigenvalue is the normal vector for the patch, and the corresponding curvature value c is calculated as,

$$c = \frac{\min(\lambda_1, \lambda_2, \lambda_3)}{\lambda_1 + \lambda_2 + \lambda_3} \quad (1)$$

Given an index i , curvature c_i and normal vector v_i of point p_i in $P_{template}$ and P_{model} can be calculated. Let's denote $\varepsilon(i)$ and $\varphi(i)$ as the mapping functions for obtaining the curvature from point p_i and v_i respectively. The normal vectors of points in $P_{template}$ and P_{model} can then be estimated as $V_{template} = \{v_i: i = 1, \dots, M\}$ and $V_{model} = \{v_j: j = 1, \dots, N\}$. The corresponding curvature values are estimated as $C_{model} = \{c_j: j = 1, \dots, N\}$, similarly, for $C_{template}$. Using C_{model} , points set of flat surface is then collected as $P_{model}^{flat} = \{p_j: \varepsilon(j) \leq C_{ts}\}$, where C_{ts} is a threshold; and normal vector as $V_{model}^{flat} = \{v_j: \varphi(j) \leq C_{ts}\}$.

B. Feature extraction for input and template

Using the Kd-tree $T_{template}$, the points positions and normal vectors around the marker center $f_{template}$ can be collected within radius R , $P_{template}^R, V_{template}^R = \{p_i, \varphi(i): |p_i - f_{template}| \leq R\}$. T_{model} is used to search for the points and normal vectors $P_{model,j}^{flat,R}, V_{model,j}^{flat,R} = \{p_j, \varphi(j): |p_j - P_{model}^{flat}| \leq R\}$ within radius R . Construct the feature vector $h_{template}$ for $f_{template}$ by $P_{template}^R, V_{template}^R$ and traverse P_{model}^{flat} and V_{model}^{flat} to construct the feature vector h_j^{flat} by $P_{model,j}^{flat,R}, V_{model,j}^{flat,R}$. The normal vector distribution on the surface of the markers is shown in Fig. 4. Normalize these normal vectors and shift the starting points of these normal vectors to $(0,0,0)$, then the end points of the normal vectors will fall on a sphere of radius 1, as shown in Fig. 5. It can be seen that the normal vectors on the same plane have the same or similar orientation, the normal end points of the cube markers are divided into five clusters on the sphere, while the normal end points of the cylinder markers are distributed on the equator or the North Pole. From this analysis, the normal vector distribution pattern characterizes the shape of local surface centers at $f_{template}$ or P_{model}^{flat} . Take the surface where p_j^{flat} is located as an example to construct h_j^{flat} . The end point set of $V_{model,j}^{flat,R}$ is denoted as point set $S_{model,j}^{flat,R}$ after translation and normalization, and $S_{model,j}^{flat,R}$ falls on the sphere radius 1mm. Since the North Pole of the sphere needs to be in the same direction as v_j^{flat} , the sphere is first rotated in the direction according to the reference vector $z = (0,0,1)$, using (2). The rotation matrix for aligning $S_{model,j}^{flat,R}$ is calculated using (3) and (4), and applied in (5).

$$\omega_j^{flat} = z \times (v_j^{flat} - p_j^{flat}) = (w_x, w_y, w_z) \quad (2)$$

$$\theta_j^{flat} = \arccos\left(\frac{z \cdot (v_j^{flat} - p_j^{flat})}{|v_j^{flat} - p_j^{flat}| |z|}\right) \quad (3)$$

$$T_j^{flat} = \omega_j^{flat} \cos(\theta_j^{flat}) I + \sin(\theta_j^{flat}) [u]_{\times} + (1 - \cos(\theta_j^{flat}))(\omega_j^{flat} \otimes \omega_j^{flat}) \quad (4)$$

$$U_{model,j}^{flat,R} = T_j^{flat} \cdot S_{model,j}^{flat,R} \quad (5)$$

Then, a cube with edge length 2mm is generated for analyzing the aligned normal vector field. The center of cube is moved to origin, overlaps with the sphere of normal vector. It is further divided into 27 ($3 \times 3 \times 3$) "bins" of equal size. The aligned normal vector end points $U_{model,j}^{flat,R}$ are then grouped into the bins for generating feature vector. Number of points in each bin is counted, and a 27-dimensional feature vector h_j^{flat} is further generated with the bin count.

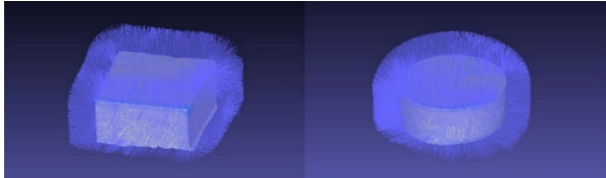


Fig. 4. The normal vector of the markers.

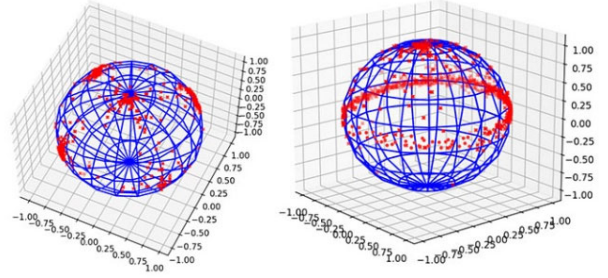


Fig. 5. Distributions of normal vector, left: CC, right: disc.

C. Geometric markers detection

When the distance of the local feature vectors h_j^{flat} to $h_{template}$ is minimum, the corresponding marker is said located at index j . According to the cosine similarity and Pearson correlation coefficient [20], the index j of the eigenvector most similar to $h_{template}$ can be calculated from the set of eigenvectors, as shown in (6). Then, $P_{marker} = \{p_j: |p_j - p_j| \leq R\}$ represents the set of points of the marker in the model.

$$J = \arg \max_{j \in N} \left(\frac{(h_j^{flat} - \overline{h_j^{flat}}) \cdot (h_{template} - \overline{h_{template}})}{|h_j^{flat} - \overline{h_j^{flat}}| |h_{template} - \overline{h_{template}}|} \right) \quad (6)$$

D. Alignment to the coordinate axes

The orthogonal planes of $P_{markerCC}$ were cut out by using RANSAC method with plane model. The points along the edges are used to calculate the orthogonal unit vector respectively for target axes X,Y,Z: $x = (x_1, x_2, x_3)^T$, $y = (y_1, y_2, y_3)^T$ and $z = (z_1, z_2, z_3)^T$. p^{origin} is also found by the intersection point of the orthogonal planes, which is used to translate the input point cloud to the origin. The alignment matrix is then given by $T_{align} = [x \ y \ z]^T$. Denote the input original point cloud as $p^{before} = \{p_r^{before}: r = 1, \dots, R\}$, and the registered model point set is denoted as $p^{after} = \{p_r^{after}: r = 1, \dots, R\}$, where R is the number of the pointset. The alignment can be done by, $p_r^{after} = T_{align} \cdot (p_r^{before} - p^{origin})$. The registration result is shown in Fig. 6.

IV. EXPERIMENT

In this section, we are going to see the performance of the proposed registration method. CMM measurements of the implant tips are used as the gold standard for this experiment. The model with the labeled stent can be physically aligned to a CMM and the coordinates of the implant apex Q_{apex}^{CMM} and neck Q_{neck}^{CMM} were measured. The apex of the implant in the virtual domain is labeled as Q_{apex} and the neck is labeled Q_{neck} , as shown in Fig.7. Three CMM measurements were performed for each subject. Denote the results obtained from the 3D mesh model acquired using CBCT, intraoral and lab scanner on resin casts as resin-CBCT, resin-Primescan and resin-Lab respectively; using lab scan on stone model as stone-Lab.

The semi-automatic registration method is as follows: 1) select facets on the superior surface of CC and the disc in MeshLab; 2) Apply "Rotate to fit to a plane"; 3) manually translate the origin to CC and rotate to correct orientation. A reference implant mesh model was then used to align to the input image's implant hence the apex and neck of implant, $Q_{apex}^{aligned}$ and $Q_{neck}^{aligned}$, can be computed. In the experiment,

semi-auto method, the proposed method with and with using disc are compared. Experimental results are shown in Fig. 8, 9, 10 and 11 respectively for resin-CBCT, resin-Primescan, resin-Lab and stone-Lab. In the current study, implant positions were measured with CMM and used as gold standard for benchmarking. The TRE is therefore the distance between the detected implant position in virtual computerized domain and the measurement from CMM. The corresponding results of automatic registration with CC achieves mean TRE 0.50 mm, 0.36 mm, 0.43 mm, 0.46 mm; and CC with discs achieves mean TRE 0.43 mm, 0.37 mm, 0.44 mm and 0.48 mm. In semi-auto registration, it achieves mean TRE 0.52mm, 0.53mm, 0.52mm and 0.50mm.

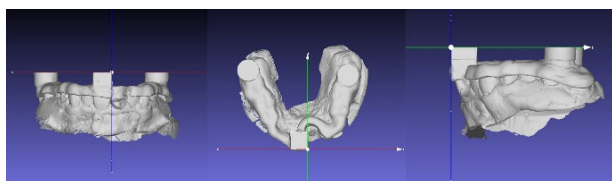


Fig. 6. The registration result in 3 orthogonal views.

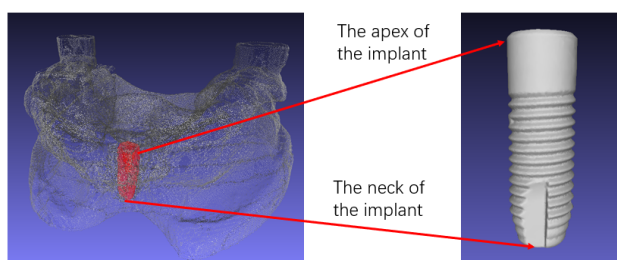


Fig. 7. The implant in the model.

V. CONCLUSION

The proposed geometric coordination registration based on multiple surfaces achieves consistently better alignment results than semi-automatic method. It can work both on CBCT and OS scans. It is automatic so that operator variability can be eliminated. When space is allowed for fabricating discs, the registration error is even much smaller, particular CBCT.

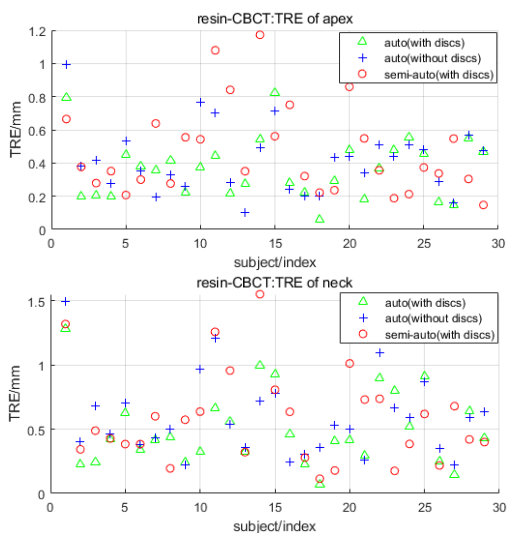


Fig. 8. TRE of resin-CBCT using the proposed and semiauto methods.

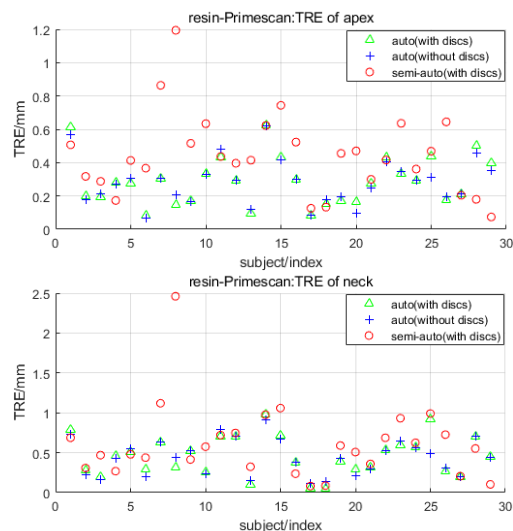


Fig. 9. TRE of resin-Primescan using the proposed and semiauto methods.

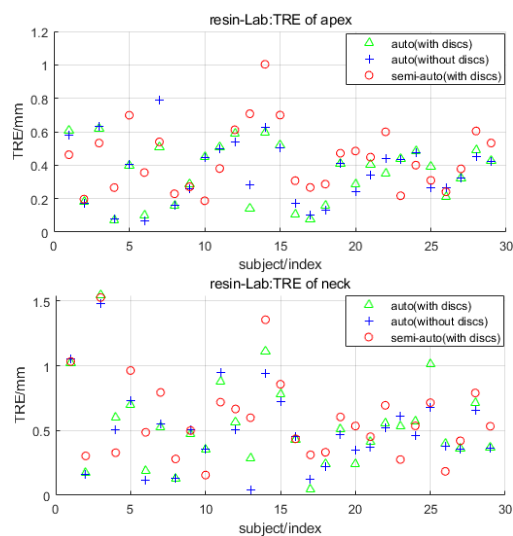


Fig. 10. TRE of resin-Lab using the proposed and semiauto methods.

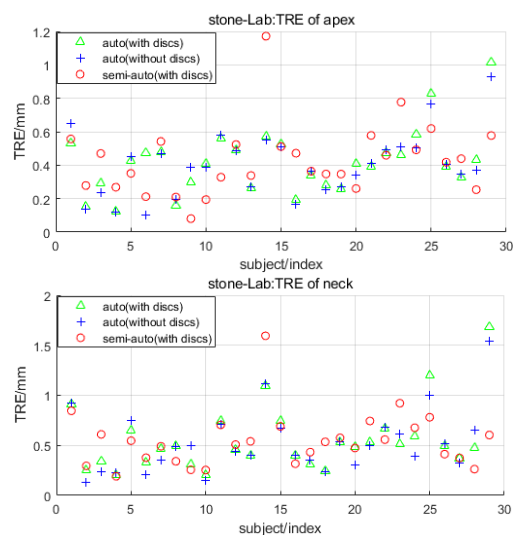


Fig. 11. TRE of stone-Lab using the proposed and semiauto methods.

COMPLIANCE WITH ETHICAL STANDARDS

This study has been approved by the HKU/HA Hong Kong West Institutional Review Board (UW 20-440).

ACKNOWLEDGMENT

This work is supported by the National Natural Science Foundation of China (No.U1701266) and Guangdong Provincial Key Laboratory of Intellectual Property and Big Data under Grant 2018B030322016.

REFERENCES

- [1] T. Albrektsson, G.A. Zarb, P. Worthington and A.R. Eriksson, "The long-term efficacy of currently used dental implants: A review and proposed criteria of success," *The International journal of oral & maxillofacial implants*, vol. 1, no. 1, pp. 11-25, 1986.
- [2] T. Albrektsson, P.I. Brånemark, H.A. Hansson, B. Kasemo, K. Larsson, I. Lundström, D.H. McQueen and R. Skalak, "The interface zone of inorganic implants In vivo: Titanium implants in bone," *Annals of Biomedical Engineering*, vol. 11, no. 1, pp. 1-27, 1983.
- [3] D. Buser, W. Martin and U.C. Belsler, "Optimizing esthetics for implant restorations in the anterior maxilla: anatomic and surgical considerations," *The International journal of oral & maxillofacial implants*, vol. 19, no. 7, pp. 43-61, 2004.
- [4] T.C. Hsung, J. Lo, T.S. Li and L.K. Cheung, "Automatic detection and reproduction of Natural Head Position in stereo-photogrammetry", *PLoS ONE*, vol. 10, no. 6, pp. e0130877, 2015.
- [5] Y.H. Lam, T.C. Hsung, W.S. Choi, W.K. Luk and H.N. Pow, "A 2-part facebow for CAD-CAM dentistry," *The Journal of Prosthetic Dentistry*, vol. 116, no. 6, pp. 843-847, 2016.
- [6] Y.H. Lam, T.C. Hsung, W.S. Choi, W.K. Luk and H.N. Pow, "A clinical technique for virtual articulator mounting with natural head position using calibrated stereophotogrammetry," *The Journal of Prosthetic Dentistry*, vol. 119, no. 6, pp. 902-908, 2018.
- [7] D.C. Hatcher, "Operational principles for cone-beam computed tomography," *The Journal of the American Dental Association*, vol. 141, supplement 3, pp. 3S-6S, 2010.
- [8] G. Frisardi, G. Chessa, S. Barone, A. Paoli, A. Rationale and F. Frisardi, "Integration of 3d anatomical data obtained by CT imaging and 3d optical scanning for computer aided implant surgery," *BMC Medical Imaging*, vol. 11, pp. 5, 2011.
- [9] S. Hassfeld and J. Muhling, "Computer assisted oral and maxillofacial surgery--a review and an assessment of technology," *International Journal of Oral Maxillofac Surgery*, vol. 30, no. 1, pp.2-13, 2001.
- [10] D.H. Zheng, Y.Z. Shen and C. Liu, "3D laser scanner and its effect factor analysis of surveying error," *Engineering of Surveying and Mapping*, vol. 14, no. 2, pp. 32-34, 2005.
- [11] Y. H. Lam, Y.T. Ngan, Y.P. Wat, W.K. Luk, H.N. Pow and T.K. Goto, "Novel geometric coordination registration in cone-beam computed Tomogram," *2014 IEEE Applied Imagery Pattern Recognition Workshop (AIPR)*, pp. 1-6, 2014.
- [12] Y.H. Lam, Y.T. Ngan, T.C. Hsung, W.K. Luk, T.K. Goto and H.N. Pow, "Validation of a novel geometric coordination registration using manual and semi-automatic registration in cone-beam computed tomogram," *Electronic Imaging*, vol. 2016, no. 14, pp. 1-6, 2016.
- [13] Y.H. Lam, Y.T. Ngan, Y.P. Wat, W.K. Luk, T.K. Goto and H.N. Pow, "Image calibration and registration in cone-beam computed tomogram for measuring the accuracy of computer-aided implant surgery," *Proceedings of SPIE, Image Processing: Machine Vision Applications VIII*, vol. 9405, pp. 60-71, 2015.
- [14] Y.H. Lam, Y.T. Ngan, T.C. Hsung, W. K. Luk, T.K. Goto and H.N. Pow, "Multiple surfaces for physical-to-image/image-to-physical registration and image verification," PCT Patent application No.PCT/CN2017/074580, International Publication No. WO2018152742, CN110462681, 2017.
- [15] J.M. Fitzpatrick, J.B. West and C.R. Maurer, "Predicting error in rigid-body point-based registration," *IEEE Transactions on Medical Imaging*, vol. 17, no. 5, pp. 694-702, 1998.
- [16] C.R. Maurer, J.M. Fitzpatrick, M.Y. Wang, R.L. Galloway, R.J. Maciunas and G.S. Allen, "Registration of head volume images using implantable fiducial markers," *IEEE Transactions on Medical Imaging*, vol. 16, no. 4, pp. 447-462, 1997.
- [17] M.F. Adnan, M.F. Daud and M.S. Saud, "Contextual Knowledge in Three Dimensional Computer Aided Design (3D CAD) Modeling: A Literature Review and Conceptual Framework," *2014 International Conference on Teaching and Learning in Computing and Engineering*, pp. 176-181, 2014.
- [18] P. Cignoni, M. Callieri, M. Corsini, M. Dellepiane, F. Ganovelli, G. Ranzuglia, "MeshLab: an Open-Source Mesh Processing Tool," *Sixth Eurographics Italian Chapter Conference*, pp. 129-136, 2008.
- [19] A. Moore, "An introductory tutorial on kd-trees," *Robotics Institute, Carnegie Mellon University, Pittsburgh*, Computer Laboratory, University of Cambridge, Technical Report no. 209, 1991.
- [20] N. Dharaneeshwaran, S. Nithya, A. Srinivasan and M. Senthilkumar, "Calculating the user-item similarity using Pearson's and cosine correlation," *International Conference on Trends in Electronics and Informatics (ICEI)*, pp. 1000-1004, 2017.